7-1-2016

Retinal Ganglion Cell and Inner Plexiform Layer Loss Correlate with Visual Acuity Loss in LHON: A Longitudinal, Segmentation OCT Analysis.

Stephen J Moster
Neuro-Ophthalmology Department, Wills Eye Hospital, Departments of Ophthalmology and Neurology, Sidney Kimmel Medical College of Thomas Jefferson University

Mark L Moster
Neuro-Ophthalmology Department, Wills Eye Hospital, Departments of Ophthalmology and Neurology, Sidney Kimmel Medical College of Thomas Jefferson University

Molly Scannell Bryan
Department of Public Health Sciences, Biological Sciences Division, University of Chicago

Robert C Sergott
Neuro-Ophthalmology Department, Wills Eye Hospital, Departments of Ophthalmology and Neurology, Sidney Kimmel Medical College of Thomas Jefferson University, robert.sergott@jefferson.edu

Retinal Ganglion Cell and Inner Plexiform Layer Loss Correlate with Visual Acuity Loss in LHON: A Longitudinal, Segmentation OCT Analysis

Stephen J. Moster,[1] Mark L. Moster,[1] Molly Scannell Bryan,[2] and Robert C. Sergott[1]

[1]Neuro-Ophthalmology Department, Wills Eye Hospital, Departments of Ophthalmology and Neurology, Sidney Kimmel Medical College of Thomas Jefferson University, Philadelphia, Pennsylvania, United States
[2]Department of Public Health Sciences, Biological Sciences Division, University of Chicago, Chicago, Illinois, United States

Correspondence: Robert C. Sergott, Wills Eye Hospital, 840 Walnut Street, Suite 930, Philadelphia, PA 19107, USA;
Rcs220@comcast.net.

Submitted: May 23, 2015
Accepted: May 15, 2016

Citation: Moster SJ, Moster ML, Scannell Bryan M, Sergott RC. Retinal ganglion cell and inner plexiform layer loss correlate with visual acuity loss in LHON: a longitudinal, segmentation OCT analysis. *Invest Ophthalmol Vis Sci*. 2016;57:3872–3883.
DOI:10.1167/iovs.15-17328

Purpose. Describe changes in the retina as vision loss progresses in Leber's Hereditary Optic Neuropathy (LHON) using spectral-domain optical coherence tomography (SD-OCT) autosegmentation, and determine if relationship exists between retinal changes and vision loss.

Methods. From patient records we identified nine LHON patients who underwent periodic neuro-ophthalmologic examinations and high-resolution SD-OCT as part of their care. We describe the impact of LHON progression on each retinal layer, and the relationship between these structural changes and visual acuity using generalized estimating equations and nonparametric tests.

Results. The thickness of the ganglion cell layer (GCL) and inner plexiform layer (IPL) decreased immediately or soon after symptom onset, and this decrease was associated with worsening vision: in the GCL a 1-mm^3 volume loss was associated with a 3.2 increase in logMAR visual acuity (95% confidence interval [CI]: 2.1–4.1); in the IPL a 1-mm^3 volume loss was associated with a 4.9 increase in visual acuity (95%CI: 6.5–3.2). The retinal nerve fiber layer (RNFL) also thinned, but not until after the GCL and IPL, and only in the papillomacular bundle (PMB) and temporal layers was thinning associated with vision loss.

Conclusions. For the first time these analyses describe a structure-function relationship between the retinal changes that occur in LHON patients as their disease progresses and vision worsens. The structural changes in the GCL, IPL, and RNFL preceded structural changes in the other retinal layers. This analysis suggests that the first 6 months after diagnosis define a target for therapeutic intervention, and this can inform treatment guidelines for ongoing therapeutic trials.

Keywords: Leber's hereditary optic neuropathy, optical coherence tomography, ganglion cell

Leber's Hereditary Optic Neuropathy (LHON) is a mitochondrially inherited disorder characterized by progressive bilateral central vision loss. Ninety percent of cases are due to three mitochondrial DNA point mutations that disrupt oxidative phosphorylation, leading to the death of retinal ganglion cells.[1] Leber's Hereditary Optic Neuropathy preferentially affects smaller axons, such as the papillomacular bundle (PMB).[2] In patients who develop decreased vision, the loss often begins unilaterally and progresses painlessly over days to weeks to levels of 20/200 or worse.[1,3] Most patients will develop vision loss in the second eye within 8 weeks, with approximately 97% of patients having involvement of both eyes within 1 year.[3,4] Occasionally some visual recovery occurs.[4–7] Penetrance is incomplete, with approximately 25% of male mutation carriers and 5% of female mutation carriers developing symptoms over their lifetime.[4,8,9] This incongruence may be related to multiple factors, including heteroplasmy, threshold expression, and a protective effect of estrogen on cells with dysfunctional mitochondria.

Strong evidence exists that the retinal structures change around the time of the onset of symptoms, although the precise nature of these changes still remains incompletely characterized. Both swelling and atrophy in retinal structures have been reported.[10–12] Many previous investigations have used time-domain optical coherence tomography (TD-OCT) to describe the retinal structures, but the resolution and reproducibility of TD-OCT measurements is quite limited.[2,13] Additionally, evidence has emerged that structural changes in the retina are associated with vision loss, although there is conflicting evidence for whether changes in the retinal nerve fiber layer (RNFL), the ganglion cell layer (GCL), or both are the initial indicators of the vision loss.[10–12,14] This research has not yet established whether swelling or thinning is associated with vision loss, and has not determined whether the changes precede or follow the vision loss.

If there is a causal relationship between structural changes and vision loss, this may present a therapeutic window in which intervening to halt the structural changes might preserve vision in LHON patients.[10] Recent advances in Spectralis OCT have allowed for SD-OCT measurements that have improved resolution, decreased variability, and an automated algorithm to quantify the retinal layers. These higher-resolution measure-

Investigative Ophthalmology & Visual Science

Table 1. Patient Characteristics

Age	
Median (interquartile range)	29 (19)
Mutation type (*n*)	
3460	1
11778	5
14484	3
Baseline symptoms (*n*)	
No eyes symptomatic at baseline	1
1 eye symptomatic at baseline	3
2 eyes symptomatic at baseline	5
Number of SD-OCT examinations (*n*)	
1 exam	2
2 exams	3
3 exams	2
4 exams	1
5 exams	1

ments have not yet been applied to examine the structure of the retina as LHON progresses.

The primary objective of our study was to use the high-resolution Spectralis SD-OCT system (software version 5.3.2; Heidelberg Engineering, Heidelberg, Germany) to quantify the thickness of the sublayers in the RNFL, GCL, inner plexiform layer (IPL), inner nuclear layer (INL), outer plexiform layer (OPL), and outer nuclear layer (ONL), and the volume of each of these layers, in the months surrounding the onset of symptoms in LHON patients. The secondary objective of our study was to establish a relationship between any changes in the retinal structures and visual acuity. Taken together, our longitudinal analyses may identify a therapeutic window and target where interventions that halt retinal changes may be applied to preserve visual function in LHON patients before atrophic changes develop.

Methods

Subjects

We conducted a chart review and identified nine consecutive unrelated LHON patients seen at the Wills Eye Hospital Neuro-Ophthalmology Service (Philadelphia, PA, USA) between December 2010 and April 2013. All had LHON mutation status determined by Athena laboratories.[15] Participants were to be excluded due to a co-occurrence of glaucoma, macular degeneration, 6 diopters (D) or more of myopia, hyperopia, high IOP, or cataract surgery. None of the nine patients met these exclusion criteria. At baseline and as part of their clinical follow-up, these patients underwent periodic neuro-ophthalmologic examinations and SD-OCT imaging. Patients were followed clinically for up to 2 years. This retrospective cohort study follows the tenets of the Declaration of Helsinki, and the study received approval from the institutional review board of Wills Eye Hospital.

Assessment of Retinal Characteristics Using Spectral-Domain OCT

To measure retinal characteristics, we implemented high-resolution SD-OCT (Spectralis). The automated retinal segmentation measured the optic nerve head and posterior pole retinal thickness, identified each retinal layer, and quantified their thicknesses and the total volume. For the RNFL, SD-OCT calculated a thickness for the superior, temporal, PMB, inferior, and nasal layers. For each of the GCL, INL, IPL, ONL, and IPL, SD-OCT calculated total volume, as well as retinal thickness values for the three concentric rings at 1 (central fovea), 3 (inner/parafoveal ring), and 6 mm (outer/perifoveal ring), breaking the inner and outer rings into four quadrants (nasal, superior, temporal, and inner), creating nine total measurements per retinal layer, corresponding to the Early Treatment Diabetic Retinopathy Study areas.[16]

The assessments were performed by our technician using a method certified in multiple clinical trials. Scans were repeated three times and only high-quality (Q values $>$ 20) scans were

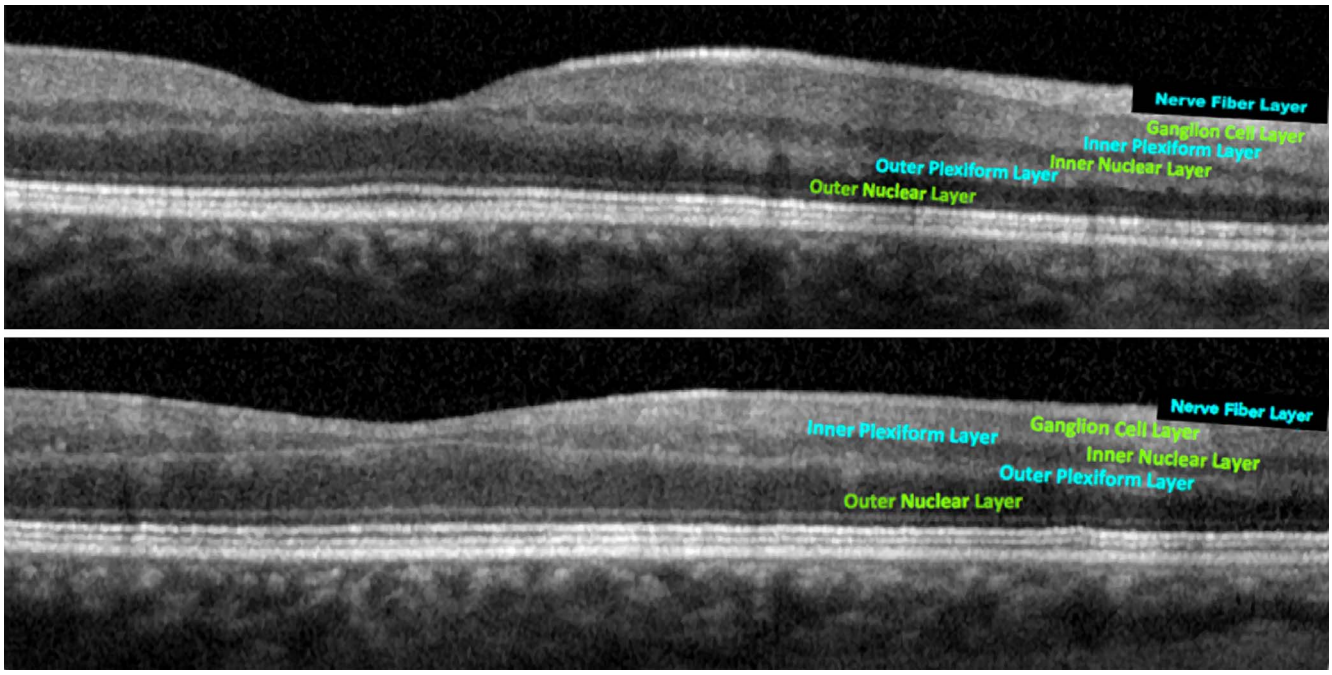

Figure 1. Topographic results of retinal layer segmentation during presymptomatic stage (*top*) and 3 months after onset (*bottom*).

Investigative Ophthalmology & Visual Science

Table 2. GEE Estimates for the Effect of Time on the Volume of the Retinal Layers, and the Effect of Volume of the Retinal Layers on Visual Acuity

	Volume Over Time			Visual Acuity as a Function of Volume		
	Estimated Change in Volume Per Month, mm^3	Standard Error	95% Confidence Interval	Estimated Effect of 1-mm^3 Increase in Volume on logMar Visual Acuity	Standard Error	95% Confidence Interval
GCL	−0.0181	0.0030	(−0.024, −0.01238)*	−3.19	0.50	(−4.11, −2.12)*
IPL	−0.0104	0.0018	(−0.0142, −0.00697)*	−4.88	0.86	(−6.51, −3.17)*
INL	0.0027	0.0010	(0.00068, 0.00462)*	1.43	1.87	(−2.39, 4.76)
OPL	0.0011	0.0016	(−0.00193, 0.00452)	1.26	1.39	(−1.31, 4.12)
ONL	0.0021	0.0029	(−0.00365, 0.00762)	1.63	0.54	(0.42, 2.63)*

Slopes that are significant at the $P < 0.05$ level are marked with an asterisk.

included. Segmentation results were manually adjusted to ensure accuracy.

Assessment of Visual Acuity and Ophthalmologic Exam

During the neuro-ophthalmologic examination, the patients were examined to assess their pupils, retina, color vision, IOP, and a Humphrey 24-2 visual field examination was performed. Best corrected visual acuity (BCVA) was measured with a Snellen chart, and visual acuities were analyzed using logMAR methods.[17]

Statistical Analysis

Qualitatively, we described the relationships between thickness and volume of retinal structures as a function of time, and described visual acuity as a function of thickness and volume, with scatterplots fitted with a locally weighted regression (LOESS) smoothed nonparametric regression line.[18]

Quantitatively, we described the structural changes of each retinal layer over the follow-up period by implementing a generalized estimating equation (GEE) to calculate the slope of each thickness or volume over time, after accounting for age and within-patient intereye correlations. In layers where a statistically significant change was seen between retinal structure and disease duration, we used the nonparametric Wilcoxon rank sum test to identify the time period in which the median thickness first became statistically different from the thicknesses measured in presymptomatic eyes.

To quantitatively assess how changes in retinal layers were associated with visual function, we implemented a GEE to

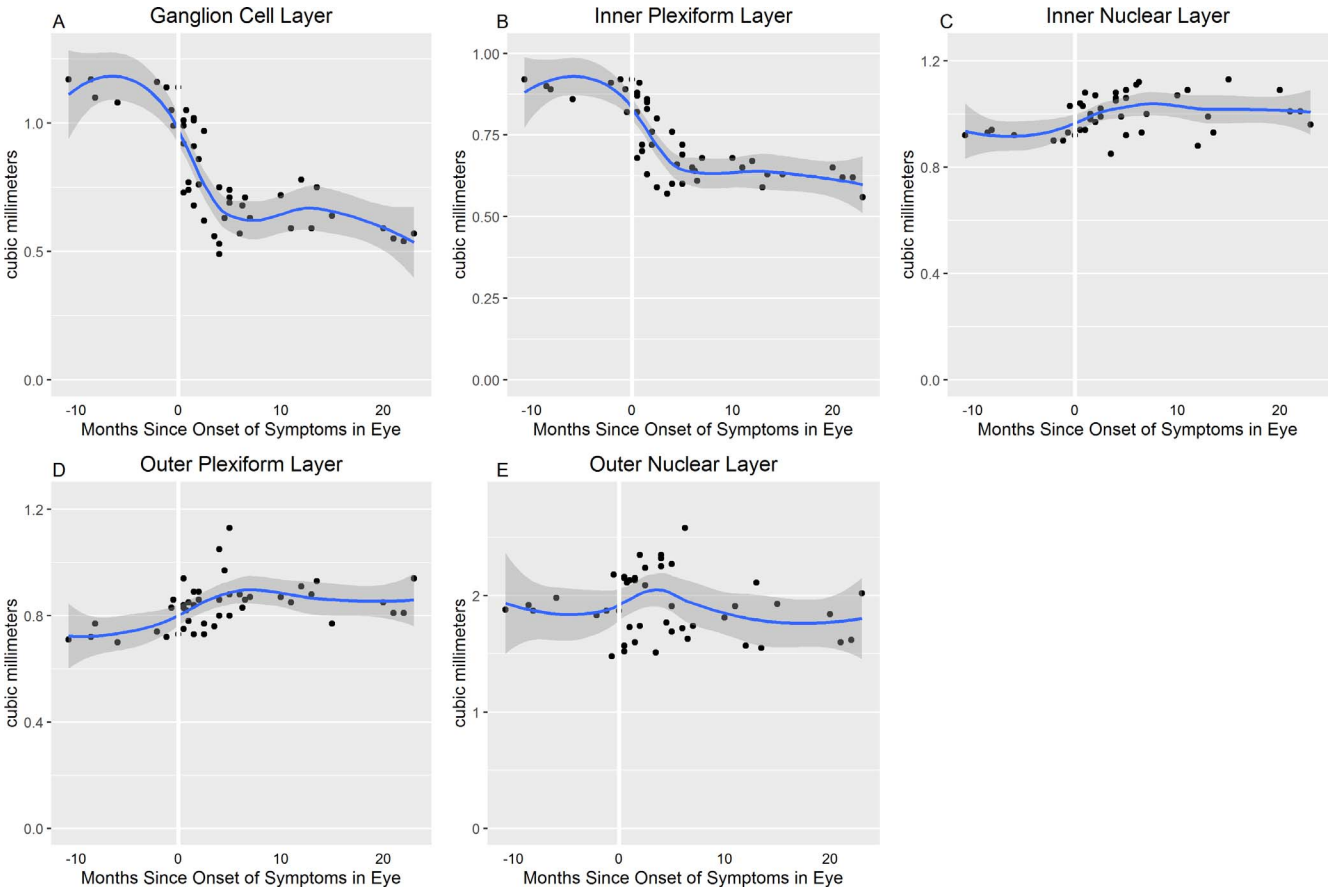

Figure 2. Macular volume during LHON progression.

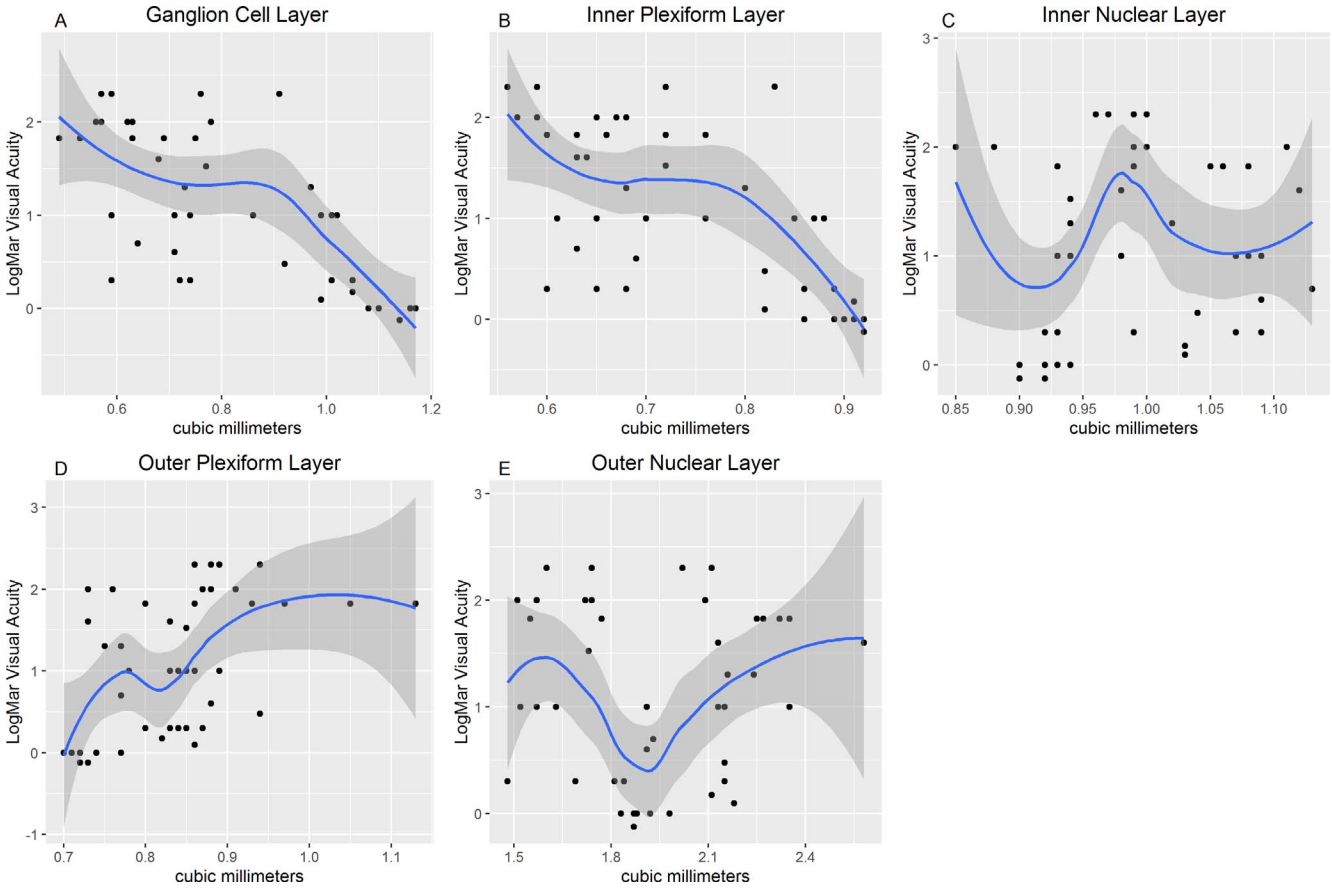

FIGURE 3. Visual acuity and macular volume.

calculate the effect of thickening or thinning of each retinal layer on visual function, after accounting for age, disease duration, and within-patient intereye correlations. Analyses were performed using R version 3.2.2.

RESULTS

Characteristics of the participants in the trial are listed in Table 1. Mutation 11778 was the most common mutation responsible for LHON, occurring in five participants, followed by mutation 14484 (three participants) and mutation 3460 (one participant). At baseline, most of the patients (five) had both eyes symptomatic, three were symptomatic in one eye, and one was symptomatic in neither eye, but developed symptoms over the course of the study. The modal patient was examined using SD-OCT twice, and the number of examinations per patient ranged from one to five. We did not observe vitreoretinal traction around the optic disk, fovea, or PMB in any patients at presentation or during follow-up.

Figure 1 displays the optical output of a typical SD-OCT scan in the same participant before the onset of symptoms in that eye (top panel) and 3 months after the onset of symptoms (bottom panel). All layers showed architectural changes as LHON progressed, as discussed in detail below.

The SD-OCT algorithm measured the total volume of the GCL, IPL, INL, OPL, and ONL (Table 2, left; Fig. 2), which provided a summary of how changes in all components of these layers change over time. The algorithm also measured how those changes were associated with visual acuity (Table 2, right; Fig. 3). The volume measurements provided evidence of progressive thinning in the GCL and IPL, both of which were significantly associated with vision loss. Additionally, there was significant swelling in the INL and not statistically significant swelling in the ONL and OPL. The details of how the substructures of the RNFL, GCL, and IPL changed with time and were associated with vision loss are discussed below. The details of how the INL, OPL, and ONL changed with time are discussed in detail in the supplemental text.

Retinal Nerve Fiber Layer

The RNFL measurements demonstrated a significant thinning that occurred after the onset of symptoms in that eye (Table 3, left; Fig. 4A). The magnitude of the speed of the thinning varied from layer to layer, with the inferior layer demonstrating the most dramatic thinning, with an estimated decrease in thickness of 4 μm/month (CI −5.1 to −2.9 μm/month) and the nasal layer thinning at the slowest rate of 1.3 μm/month (CI −1.9 to −0.7 μm/month).

In order to better quantify when these changes occurred, we calculated the median thickness for measurements taken within five time windows (Table 4): 15 days before the onset of symptoms through 15 days after the onset of symptoms; 15 days after onset through 3 months after onset; 3 to 6 months after onset; 6 to 12 months after onset; and 12 to 24 months after onset. We then identified the first of these time periods when the median thickness differed from the thickness taken in presymptomatic eyes (eyes that were measured more than

Table 3. GEE Estimates for the Effect of Time on the Thickness of the Retinal Layers and the Effect of Thickness of the Retinal Layers on Visual Acuity

	Thickness Over Time			Visual Acuity as a Function of Thickness		
	Estimated Change in Thickness Per Month, μm	Standard Error	95% Confidence Interval	Estimated Effect of 10 μm increase in Thickness on logMar Visual Acuity	Standard Error	95% Confidence Interval
RNFL						
Average	−2.78	0.31	(−3.46, −2.05)*	0.0054	0.0597	(−0.1093, 0.1271)
Superior	−2.92	0.47	(−3.97, −1.93)*	0.0635	0.0384	(−0.0087, 0.1393)
Temporal	−2.50	0.37	(−3.33, −1.68)*	−0.1135	0.0479	(−0.2045, −0.0089)*
PMB	−1.49	0.31	(−2.14, −0.89)*	−0.1731	0.0548	(−0.2754, −0.0567)*
Inferior	−4.00	0.50	(−5.08, −2.85)*	−0.0098	0.0363	(−0.0798, 0.0572)
Nasal	−1.29	0.31	(−1.93, −0.65)*	0.0613	0.0591	(−0.0550, 0.1791)
GCL						
Center	−0.27	0.05	(−0.37, −0.17)*	−1.8830	0.2955	(−2.4774, −1.1825)*
Nasal inner	−1.08	0.20	(−1.48, −0.68)*	−0.4964	0.0702	(−0.6274, −0.3387)*
Nasal outer	−0.53	0.09	(−0.70, −0.35)*	−0.9244	0.1788	(−1.2601, −0.5373)*
Superior inner	−1.24	0.19	(−1.61, −0.86)*	−0.4467	0.0862	(−0.6052, −0.2582)*
Superior outer	−0.52	0.07	(−0.66, −0.38)*	−0.6718	0.2382	(−1.1099, −0.2109)*
Temporal inner	−1.18	0.20	(−1.57, −0.80)*	−0.4772	0.0773	(−0.6201, −0.3117)*
Temporal outer	−0.68	0.09	(−0.87, −0.50)*	−0.8713	0.1722	(−1.1915, −0.5304)*
Inferior inner	−1.13	0.20	(−1.52, −0.74)*	−0.5005	0.0710	(−0.6314, −0.3454)*
Inferior outer	−0.34	0.07	(−0.48, −0.21)*	−1.4572	0.2030	(−1.8447, −1.0222)*
IPL						
Center	−0.23	0.06	(−0.34, −0.13)*	−1.4548	0.2992	(−2.0195, −0.8815)*
Nasal inner	−0.71	0.12	(−0.95, −0.48)*	−0.7946	0.1227	(−1.0279, −0.5544)*
Nasal outer	−0.28	0.05	(−0.39, −0.18)*	−1.6677	0.2854	(−2.2526, −1.0420)*
Superior inner	−0.71	0.11	(−0.93, −0.50)*	−0.7630	0.1478	(−1.0348, −0.4578)*
Superior outer	−0.22	0.04	(−0.32, −0.14)*	−0.9745	0.4167	(−1.7597, −0.1699)*
Temporal inner	−0.76	0.12	(−1.01, −0.53)*	−0.6844	0.1298	(−0.9275, −0.4337)*
Temporal outer	−0.33	0.06	(−0.46, −0.22)*	−1.0438	0.2778	(−1.5663, −0.4961)*
Inferior inner	−0.68	0.11	(−0.90, −0.47)*	−0.8576	0.1344	(−1.1055, −0.5803)*
Inferior outer	−0.24	0.03	(−0.31, −0.18)*	−2.3677	0.4748	(−3.3115, −1.2884)*

Slopes that are significant at the $P < 0.05$ level are marked with an asterisks.

15 days before the onset of symptoms).The thinning in the temporal layer was the first to reach statistical significance, with the median thickness of eyes measured between 15 days and 3 months after the onset of symptoms reaching 73 μm (confidence interval [CI]: 57–87 μm), compared with 90 μm at baseline (CI: 75–108 μm). The next layers to demonstrate significant thinning were the PMB and inferior layers measured in eyes 3 to 6 months after the onset of symptoms. By 12 to 24 months after onset, all layers were significantly different from baseline, with the average median thickness decreased by more than half in most layers.

In the PMB and the temporal layers, we found evidence that the thinning observed was associated with changes in visual acuity (Fig. 5; Table 3, right). In the PMB layer, a 10-μm thinning was associated with a 0.173 increase in logMAR visual acuity (CI: –0.275 to 0.057 logMAR/μm), and in the temporal layer, 1-μm thinning was associated with a 0.113 increase in visual acuity.

Ganglion Cell Layer

All layers in the GCL showed significant thinning over time, and that thinning was associated with a loss of vision (Tables 3, 5). A qualitative examination of the thickness of the GCL (Fig. 6) suggests that the thinning in the GCL occurred around the time of disease onset, and then stabilized at approximately 6 months. As with the RNFLs, each layer individually demonstrated a thinning that is statistically significant at the $\alpha = 0.05$ level (Table 3, left), with the most rapid thinning occurring in the superior inner layer (1.24 μm/month; CI: –1.61 to –0.86 μm/month), followed by the temporal inner (1.18 μm/month; CI: –1.57 to –0.8 μm/month), and inferior inner (1.13 μm/month; CI: –1.52 to –0.74 μm/month) layers.

There is evidence that the thinning in the GCL occurred possibly before the thinning in the RNFL, because in some layers the thinning was statistically different from presymptomatic eyes sooner (Table 5). In the temporal inner and inferior outer layers, the median measurements taken concurrent with the onset of symptoms were already significantly different from measurements taken before symptoms developed. By 3 months after symptoms developed in the eye, 7 of 9 layers were significantly thinner than predisease in measurements, and all layers were different from baseline by 6 months after disease onset.

The thinning observed in all layers of the GCL was correlated with worsening eyesight (Fig. 7; Table 3, right). Thinning in the center layer of the GCL was estimated to have the largest impact on visual acuity with 10-μm thinning associated with a 1.9 increase in logMAR visual acuity (CI: –2.5 to –1.2), followed by the inferior outer layer (10-μm thinning associated with a 1.5 increase in logMAR visual acuity (CI: –1.8 to –1.0).

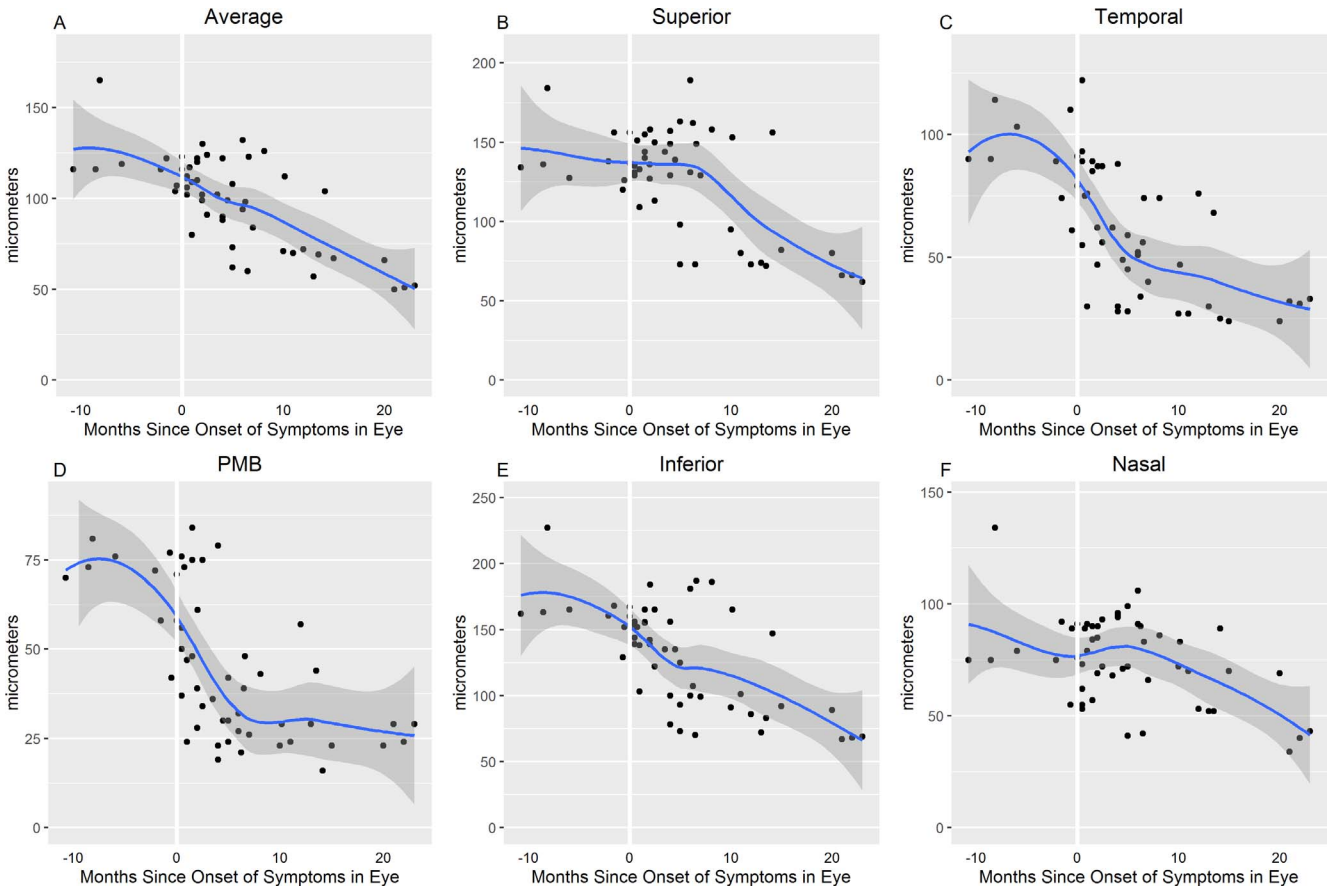

Figure 4. Retinal nerve fiber layer thickness during LHON progression.

Inner Plexiform Layer

As with the GCL, most of the thinning of the IPL occurred in the first 6 months after the onset of symptoms in the eye (Fig. 8; Table 3, left, and Table 6). The inner layers (nasal inner, superior inner, temporal inner, and inferior inner) showed a larger decrease in magnitude than the outer layers (Table 3, left). The magnitude of the thinning in the IPL was less than in the GCL.

The inferior inner layer of the IPL showed significant thinning at the time of the onset of symptoms, thinning to 37 μm (CI: 29–42 μm) at the time of disease onset compared with 43 μm at baseline (CI: 39–43 μm; Table 6). The nasal inner, nasal outer, superior inner, temporal inner, and inferior outer layers were all significantly thinned when compared with baseline by 3 months after the disease onset, and all nine layers were significantly thinned by 6 months after the onset of symptoms.

The thinning observed in the IPL was associated with worse eyesight, with all layers demonstrating a negative association between thickness and logMAR visual acuity (Fig. 9; Table 3, right). When the association was compared with the one observed in the GCL, the larger standard errors of the estimates and the increased scatter of the data indicate that this association between visual acuity and the thickness of the layers is less precise in the IPL.

Table 4. Median Thickness of the Retinal Nerve Fiber Layer as Symptoms Progress

	Median (95%CI)					
	Presymptomatic Eye	0.5 mo Before Onset to 0.5 mo After Onset	0.5–3 mo After Onset	3–6 mo After Onset	6–12 mo After Onset	12–24 mo After Onset
Average	116 (110, 141)	112 (102, 123)	110 (99, 120)	97 (82, 112)*	92 (70, 112)	60 (51, 85)*
Superior	136 (126, 160)	134 (130, 146)	139 (126, 150)	140 (114, 160)	117 (80, 155)	74 (66, 115)*
Temporal	90 (75, 108)	89 (55, 122)	73 (57, 87)*	48 (37, 62)*	51 (33, 74)*	30 (24, 49)*
PMB	72 (57, 77)	57 (37, 76)	54 (36, 73)	30 (24, 51)*	34 (24, 46)*	26 (20, 36)*
Inferior	163 (146, 195)	154 (139, 167)	148 (130, 162)	117 (89, 145)*	126 (86, 165)	80 (68, 115)*
Nasal	82 (65, 106)	68 (53, 91)	83 (73, 90)	84 (68, 97)	72 (57, 85)	55 (40, 71)*

Time periods in which the median thickness differs from the thickness at baseline at the $P < 0.05$ level are marked with an asterisk.

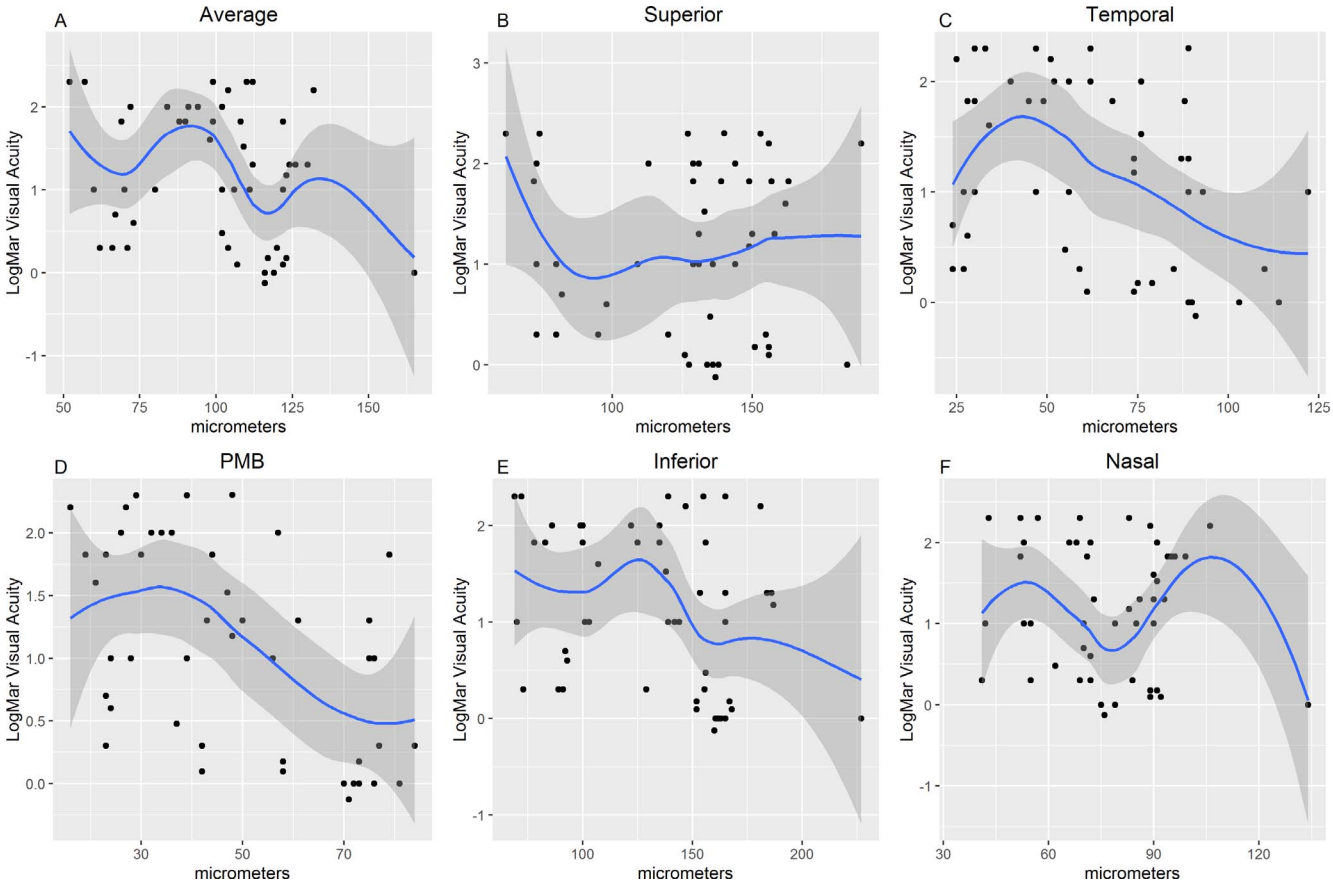

FIGURE 5. Visual acuity and RNFL thickness.

Inner Nuclear Layer, Outer Plexiform Layer, and Outer Nuclear Layer

In contrast to the GCL and the IPL, in our patients, the INL, OPL, and ONL did not thin as the disease progressed, and there is qualitative evidence that some layers thickened in the months after diagnosis (Supplementary Figs. S1, S3, S5; Supplementary Table S1, left). The thickening that was seen in the layers was not generally correlated with changes in visual acuity (Supplementary Table 3, right; Supplementary Figs. S2, S4, S6). In layers where there was an association between vision and thickness, the association was reversed from what was found in the RNFL, GCL, and IPL, with worse eyesight being associated with thickening rather than thinning.

DISCUSSION

Using the validated and consistent measurement of SD-OCT, our analysis describes the structural changes occurring in

TABLE 5. Median Thickness of the Ganglion Cell Layer as Symptoms Progress

	Median (95%CI)					
	Presymptomatic Eye	0.5 mo Before Onset to 0.5 mo After Onset	0.5–3 mo After Onset	3–6 mo After Onset	6–12 mo After Onset	12–24 mo After Onset
Center	13 (12, 15)	14 (7, 16)	12 (9, 14)	9 (7, 10)*	9 (8, 11)*	8 (7, 9)*
Nasal inner	53 (46, 55)	42 (26, 56)	31 (24, 37)*	20 (15, 24)*	22 (19, 28)*	20 (18, 26)*
Nasal outer	39 (36, 43)	33 (24, 43)	30 (26, 34)*	24 (21, 27)*	25 (23, 27)*	23 (21, 25)*
Superior inner	55 (49, 58)	48 (35, 56)	36 (29, 44)*	24 (19, 30)*	26 (21, 30)*	21 (18, 27)*
Superior outer	36 (33, 38)	33 (28, 38)	32 (28, 36)	23 (19, 28)*	25 (23, 26)*	22 (20, 24)*
Temporal inner	50 (46, 53)	40 (25, 51)	33 (24, 42)*	19 (17, 24)*	20 (15, 26)*	17 (15, 23)*
Temporal outer	37 (36, 38)	33 (26, 35)*	30 (25, 34)*	22 (20, 24)*	22 (19, 27)*	20 (17, 22)*
Inferior inner	55 (47, 58)	42 (27, 57)	34 (28, 42)*	23 (19, 29)*	28 (22, 35)*	21 (19, 28)*
Inferior outer	33 (32, 35)	30 (25, 33)*	28 (25, 31)*	25 (22, 27)*	26 (24, 29)*	23 (21, 25)*

Time periods in which the median thickness differs from the thickness at baseline at the $P < 0.05$ level are marked with an asterisk.

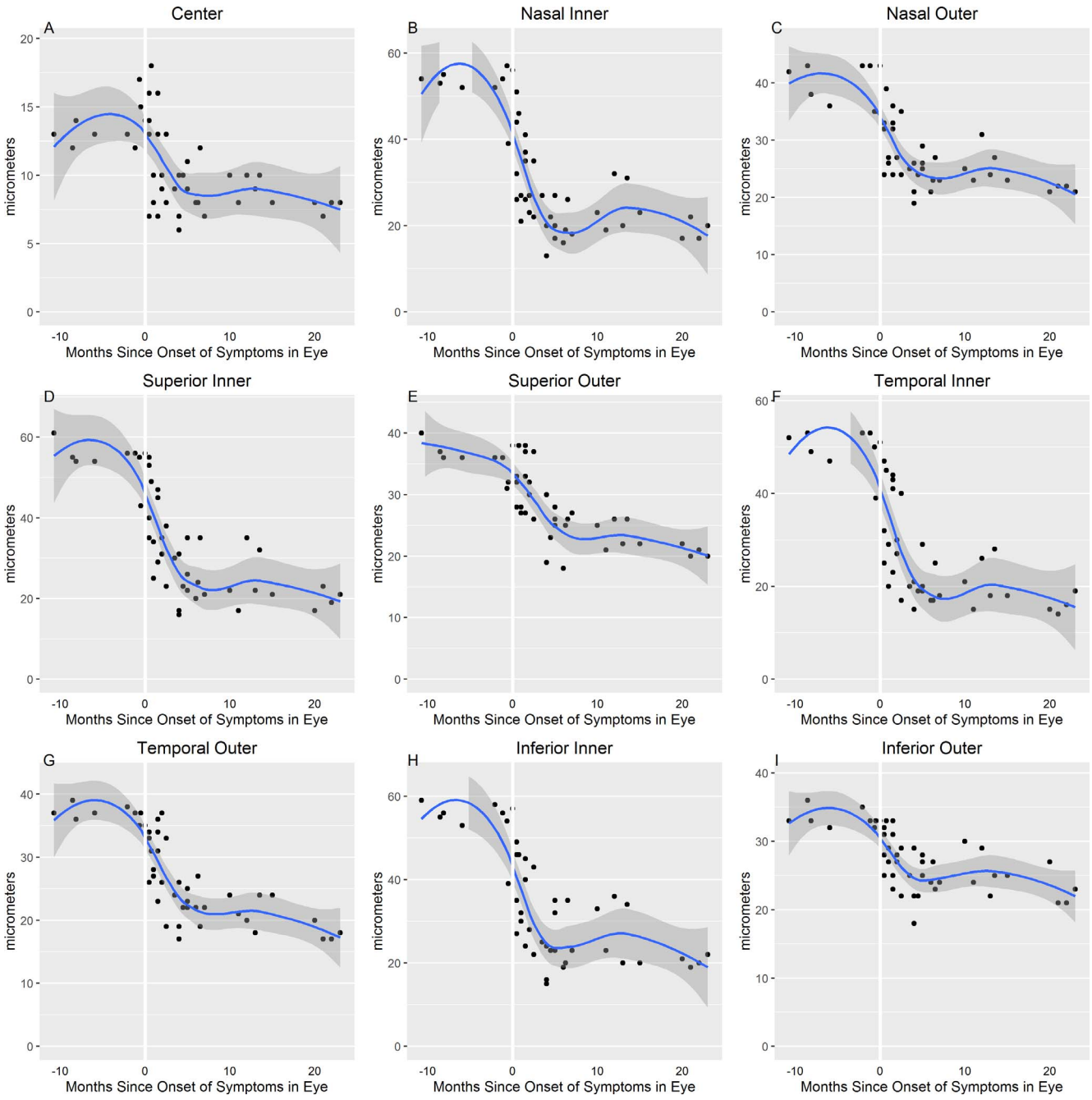

FIGURE 6. Ganglion cell layer thickness during LHON progression.

retina in the months around the onset of symptoms in LHON patients, and suggests thinning of the RNFL, GCL, and IPL, may drive part of the vision loss experienced by patients with LHON. We would recommend using GCL as an anatomic marker of therapeutic effect over RNFL, as our results show a stronger relationship between these layers and visual acuity. While our results are not inconsistent with changes in the RNFL causing vision loss, we were able to identify a significant difference in the thickness of the GCL and IPL before changes were conclusively seen in the substructures of the RNFL. Therefore, when considering evolving treatments for LHON, early treatment before RNFL shows thinning would be advised.

Our results establish that the retinal structural changes evolve during the time around onset of LHON symptoms, and suggest two distinct response patterns: progressive thinning that begins around the onset of symptoms, and slows at approximately 6 months, in which thinning is associated with vision loss; and swelling around the time of the onset of symptoms, with increasing thickness associated with vision loss; the RNFL, GCL, and IPL behave like the former, and the INL, OPL, and ONL behave like the later.

Compared with previous research, our data are consistent with reports of a relationship between visual acuity and RNFL thinning,[2] and in contrast to studies that found RNFL thickening around the time of onset.

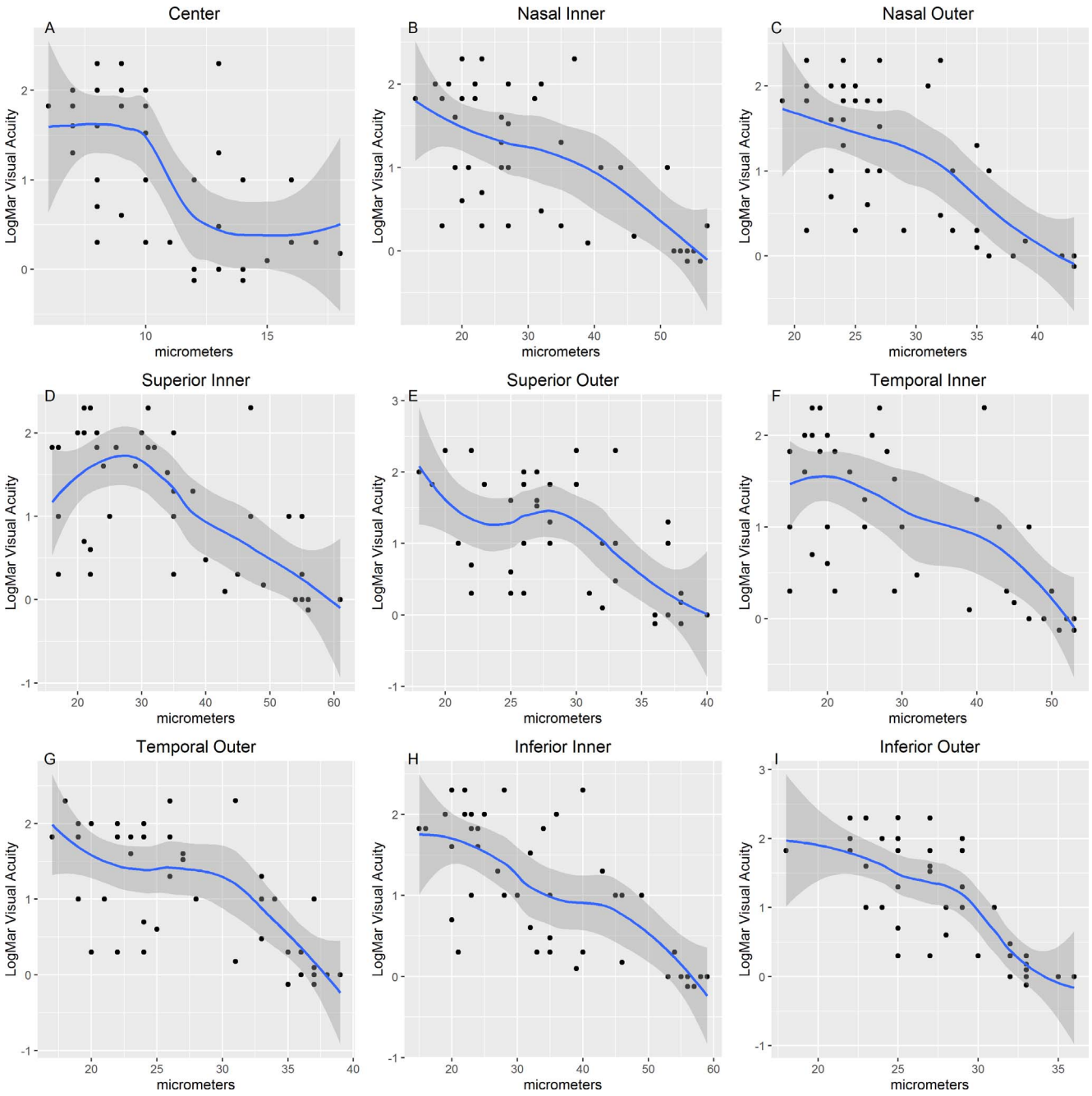

Figure 7. Visual acuity and GCL thickness.

Table 6. Median Thickness of the Inner Plexiform Layer as Symptoms Progress

	Median (95%CI)					
	Presymptomatic Eye	**Within 0.5 mo of Onset**	**0.5–3 mo After Onset**	**3–6 mo After Onset**	**6–12 mo After Onset**	**12–24 mo After Onset**
Center	19 (17, 21)	20 (16, 22)	19 (16, 21)	15 (14, 16)*	16 (15, 17)*	15 (14, 16)*
Nasal inner	42 (39, 44)	36 (28, 43)	29 (26, 34)*	25 (22, 27)*	25 (23, 27)*	22 (19, 25)*
Nasal outer	30 (28, 33)	28 (20, 32)	25 (22, 27)*	22 (21, 23)*	22 (21, 22)*	22 (21, 23)*
Superior inner	42 (38, 42)	38 (34, 43)	33 (28, 38)*	26 (22, 28)*	25 (23, 27)*	22 (22, 24)*
Superior outer	28 (26, 29)	27 (26, 28)	26 (24, 29)	23 (21, 25)*	23 (22, 25)*	22 (21, 23)*
Temporal inner	41 (39, 42)	39 (25, 44)	34 (28, 39)*	26 (22, 30)*	26 (23, 28)*	22 (18, 26)*
Temporal outer	31 (30, 32)	32 (29, 32)	29 (26, 31)	25 (21, 29)*	25 (22, 26)*	22 (20, 23)*
Inferior inner	43 (39, 43)	37 (29, 42)*	31 (27, 34)*	25 (22, 29)*	26 (24, 29)*	23 (22, 26)*
Inferior outer	27 (26, 27)	26 (24, 26)	23 (22, 25)*	23 (21, 25)*	22 (20, 23)*	20 (20, 22)*

Time periods in which the median thickness differs from the thickness at baseline at the $P < 0.05$ level are marked with an asterisk.

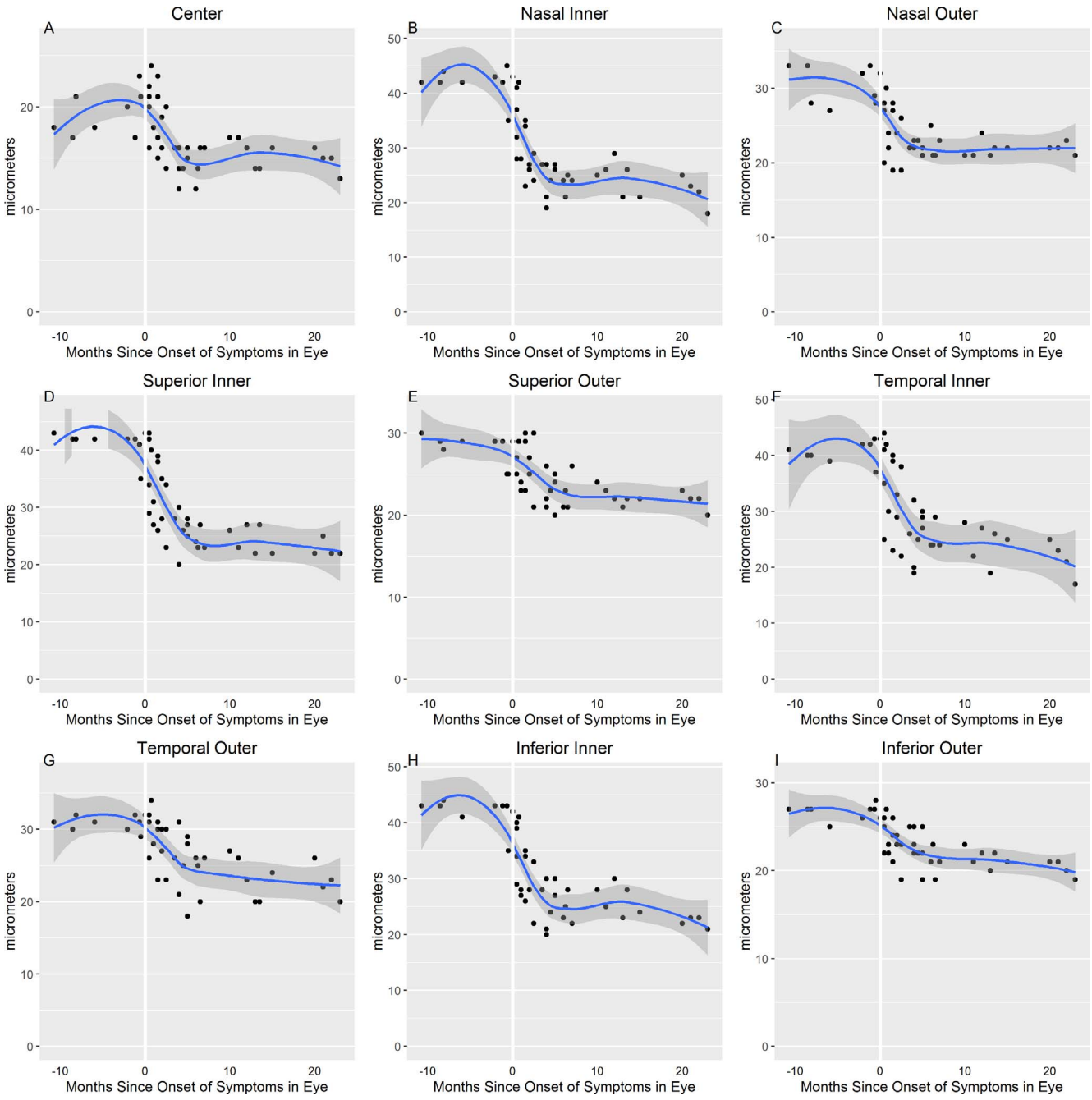

FIGURE 8. Inner plexiform layer thickness during LHON progression.

Our analysis does have some limitations. Leber's Hereditary Optic Neuropathy studies are inherently difficult due to the inability to identify which carriers will go on to have vision loss. Although the longitudinal nature of our study provided multiple observations on each subject, our study enrolled nine participants. Due to the modest sample size, the complexity of our statistical models was limited by power considerations. Although we were able to control for age and within-eye correlation, we would have additionally liked to control for other possible confounders, and we would have liked to test to see if the pattern of swelling and thinning differed by mutation status. Similarly, due to the sample size, it is possible that the assumptions of GEE are not fully met, and therefore, although GEE is still the best way to control for interperson correlation, the GEE estimates may be unstable. In addition, many patients present for evaluation only after their initial visual decline, so the presymptomatic eyes in our cohort are largely from individuals who have already experienced unilateral vision loss, which may not represent the true thickness seen in asymptomatic carriers. Additionally, our analyses tested multiple hypotheses, and therefore the reported statistical significance threshold ($\alpha = 0.05$) does not definitively establish a causal relationship. However, as the nature of our analysis is descriptive of the structural changes, we did not design our study to meet a strict significance threshold such as a Bonferroni correction.

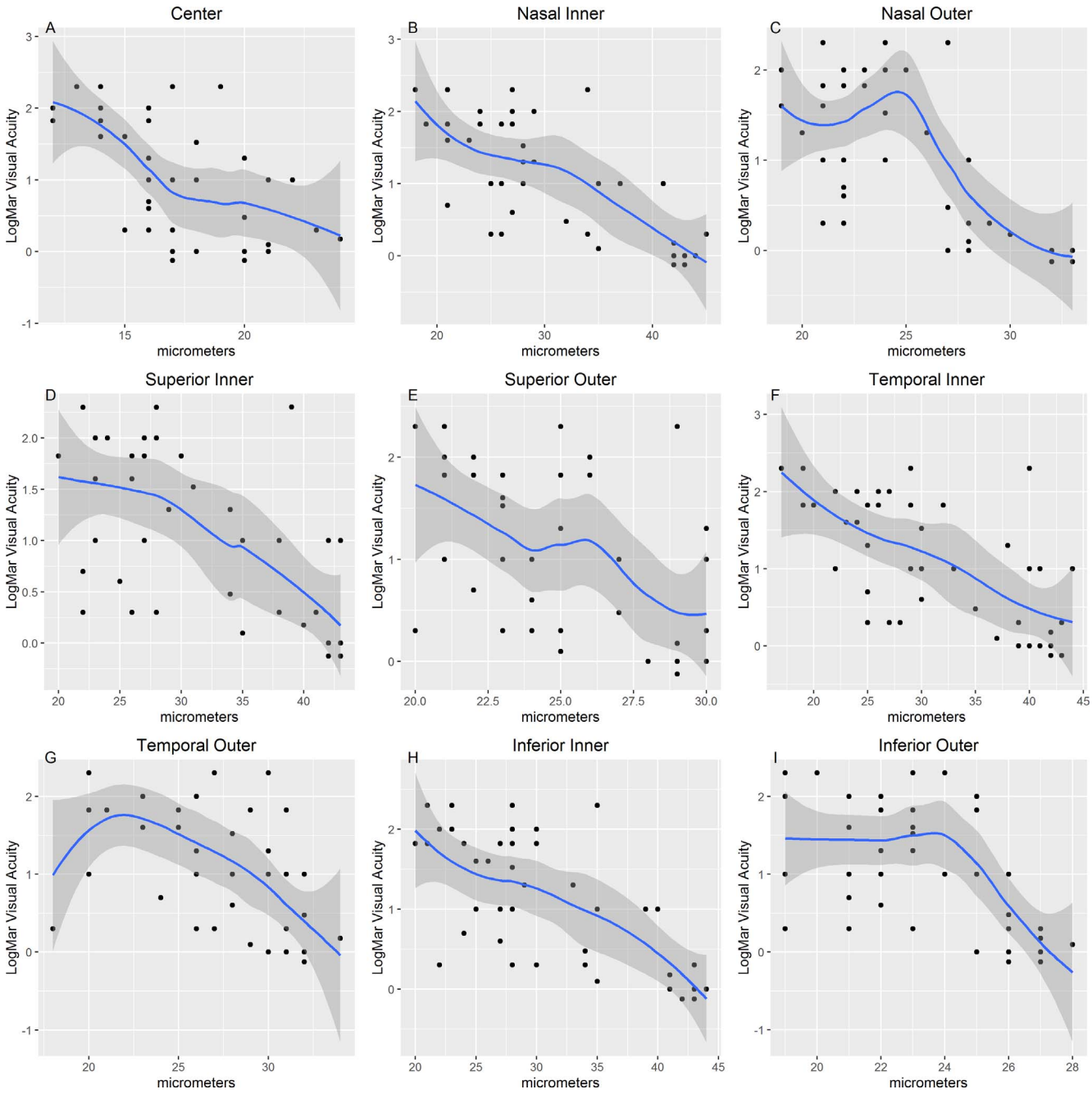

Figure 9. Visual acuity and IPL thickness.

These analyses suggest several paths for future research. Future studies to examine retinal structure changes in individuals who regain vision might provide insight in to the potential protective structural differences that are associated with this regain of function, which may further suggest therapeutic targets. It would also be of interest to see if a threshold of GCL, RNFL, or IPL loss exists in asymptomatic carriers before visual symptoms occur. Given the dramatic decline in thickness in the GCL, RNFL, and IPL, changes from an asymptomatic carriers baseline may indicate that vision loss is imminent, and present a potential therapeutic window.

In summary, our investigation uses SD-OCT to measure retinal segmentation and demonstrate a structure-function relationship between visual acuity and retinal anatomy in LHON patients. Our findings suggest that the variability in the RNFL observed by others does not translate to patterns of retinal ganglion cell death. We suggest that instead of RNFL, that thinning in the GCL and, to a lesser extent, IPL, may drive vision loss in LHON patients. In the GCL and IPL, there is strong evidence of thinning that begins at or immediately following the onset of symptoms, and the thinning is associated with vision loss. Our analyses also demonstrate the greater sensitivity of SD-OCT compared with TD-OCT, and supports the use of SD-OCT of the GCL as a secondary or coprimary endpoint in clinical trials, because there is a clear linear pattern of GCL thinning during the acute phase,

followed by relative preservation of thickness after 6 months. If these structural changes are verified to be causing the vision loss, they provide a compelling possibility for therapeutic targets to slow the progression of vision loss associated with LHON.

Acknowledgments

Disclosure: **S.J. Moster**, None; **M.L. Moster**, Gensight (F); **M. Scannell Bryan**, None; **R.C. Sergott**, Heidelberg Engineering (C)

References

1. Fraser JA, Biousse V, Newman NJ. The neuro-ophthalmology of mitochondrial disease. *Surv Ophthalmol*. 2010;55:299–334.
2. Sadun AA, Win PH, Ross-Cisneros FN, Walker SO, Carelli V. Leber's hereditary optic neuropathy differentially affects smaller axons in the optic nerve. *Trans Am Ophthalmol Soc*. 2000;98:223–232, discussion 232–225.
3. Newman NJ. Hereditary optic neuropathies. In: Miller NR, Newman NJ, ed(s). *Walsh and Hoyt's Clinical Neuro-Ophthalmology*. 6th ed. Philadelphia, PA: 2005;465–501.
4. Riordan-Eva P, Sanders MD, Govan GG, Sweeney MG, Da Costa J, Harding AE. The clinical features of Leber's hereditary optic neuropathy defined by the presence of a pathogenic mitochondrial DNA mutation. *Brain*. 1995;118(Pt 2):319–337.
5. Mashima Y, Sato EA, Ohde H, Oguchi Y. Macular nerve fibers temporal to fovea may have a greater potential to recover function in patients with Leber's hereditary optic neuropathy. *Jpn J Ophthalmol*. 2002;46:660–667.
6. Oostra RJ, Bolhuis PA, Wijburg FA, Zorn-Ende G, Bleeker-Wagemakers EM. Leber's hereditary optic neuropathy: correlations between mitochondrial genotype and visual outcome. *J Med Genet*. 1994;31:280–286.
7. Stone EM, Newman NJ, Miller NR, Johns DR, Lott MT, Wallace DC. Visual recovery in patients with Leber's hereditary optic neuropathy and the 11778 mutation. *J Clin Neuroophthalmol*. 1992;12:10–14.
8. Newman NJ, Biousse V, David R, et al. Prophylaxis for second eye involvement in Leber hereditary optic neuropathy: an open-labeled, nonrandomized multicenter trial of topical brimonidine purite. *Am J Ophthalmol*. 2005;140:407–415.
9. Lam BL, Feuer WJ, Schiffman JC, et al. Trial end points and natural history in patients with g11778a Leber hereditary optic neuropathy: preparation for gene therapy clinical trial. *JAMA Ophthalmol*. 2014;132:428–436.
10. Barboni P, Carbonelli M, Savini G, et al. Natural history of Leber's hereditary optic neuropathy: longitudinal analysis of the retinal nerve fiber layer by optical coherence tomography. *Ophthalmology*. 2010;117:623–627.
11. Barboni P, Savini G, Valentino ML, et al. Retinal nerve fiber layer evaluation by optical coherence tomography in Leber's hereditary optic neuropathy. *Ophthalmology*. 2005;112:120–126.
12. Savini G, Barboni P, Valentino ML, et al. Retinal nerve fiber layer evaluation by optical coherence tomography in unaffected carriers with Leber's hereditary optic neuropathy mutations. *Ophthalmology*. 2005;112:127–131.
13. Barboni P, Carelli V, Savini G, Carbonelli M, La Morgia C, Sadun AA. Microcystic macular degeneration from optic neuropathy: not inflammatory, not trans-synaptic degeneration. *Brain*. 2013;136(Pt 7):e239.
14. Guy J, Feuer WJ, Porciatti V, et al. Retinal ganglion cell dysfunction in asymptomatic g11778a: Leber hereditary optic neuropathy. *Invest Ophthalmol Vis Sci*. 2014;55:841–848.
15. Stone EM. Genetic testing for inherited eye disease. *Arch Ophthalmol*. 2007;125:205–212.
16. Treatment techniques and clinical guidelines for photocoagulation of diabetic macular edema. Early treatment diabetic retinopathy study report number 2. Early treatment diabetic retinopathy study research group. *Ophthalmology*. 1987;94:761–774.
17. Holladay JT. Proper method for calculating average visual acuity. *J Refract Surg*. 1997;13:388–391.
18. Cleveland WS, Devlin SJ, Grosse E. Regression by local fitting: methods, properties, and computational algorithms. *J Econ*. 1988;37:87–114.

Investigative Ophthalmology & Visual Science